Author Manuscript:
Published in final edited form as: Nuclear Instruments and Methods in Physics Research B 267 (2009) 167–170.
https://doi.org/10.1016/j.nimb.2008.10.094

Energy Dependence of Electron Stopping Powers in Elemental Solids over the 100 eV to 30 keV Energy Range

K. Kumagai*

Graduate School of Pure and Applied Science, University of Tsukuba,

1-1 Namiki, Tsukuba, Ibaraki 305-0044, Japan

S. Tanuma

Materials Analysis Station, National Institute for Materials Science, 1-2-1 Sengen, Tsukuba,

Ibaraki 305-0047, Japan

C. J. Powell

Surface and Microanalysis Science Division, National Institute of Standards and

Technology, Gaithersburg, MD, 20899-8370, USA

*Corresponding author. Tel. +81-29-859-2725 Fax. +81-29-859-2729

e-mail: kumagai.kazuhiro@nims.go.jp

Abstract

We analyzed the energy dependence of electron stopping powers (SPs) calculated for 41 elemental solids from experimental optical data for electron energies between 100 eV and 30 keV. Our analysis was performed based on the Hill equation to represent a series of steps in plots of the slopes of Fano plots. The average root-mean-square difference between SPs from fits with an equation derived from the Hill equation and the calculated SPs was 1.0 %. The

new equation can provide SPs over a wide energy range for Monte Carlo simulations of electron transport with the continuous slowing-down approximation.

Keyword: Electron stopping power; Fano plot; Elemental solids; Energy dependence

The electron stopping power (SP) is an important parameter in the modeling of electron transport in solids for many applications such as electron-probe microanalysis [1-3], Auger-electron spectroscopy [4], and dimensional metrology in the scanning electron microscope [5-7]. In Monte Carlo simulations for these and other applications, the continuous slowing-down approximation has often been utilized in which it is assumed that the electron energy is a continuous function of the trajectory length in a material. This approach is convenient because data for differential cross sections as a function of energy loss are not required and because computation time is reduced if inelastic-scattering events are not individually simulated [4]. It is, however, necessary to know the dependence of the SP on electron energy in solids over a wide energy range, typically 100 eV to 30 keV.

SPs for Monte Carlo simulations have often been determined from the Bethe SP equation [8-10] and data for one material parameter, the mean excitation energy [11]. This equation is expected to be valid for electron energies greater than about 10 keV or for energies much greater than the largest K-shell binding energy in the material of interest. SPs calculated from the Bethe equation are available from a National Institute of Standards and Technology (NIST) database for electron energies of 10 keV and above [12]. Several empirical SP equations [13-15] have been developed for energies less than 10 keV but their use is restricted to materials for which needed parameters are known. Furthermore, it is difficult to adapt these equations to energies less than several hundred eV. Although experimental determinations of the SP over a range of energies are available for a limited

number of materials [16], different sets of data for a particular material can disagree significantly.

Tanuma *et al.* [17, 18] recently reported SPs for 41 elemental solids over the 100 eV to 30 keV energy range that were calculated from experimental optical data using the Penn algorithm [19]. Jablonski *et al*. [20] analyzed these results and proposed an empirical predictive SP formula for the 200 eV to 30 keV energy range.

We report a new analysis of the calculated SPs of Tanuma *et al.* [17, 18] and propose a new SP formula that can be applied over the 100 eV to 30 keV energy range. Our analysis of the SP energy dependence for each solid was carried out using Fano plots [21, 22] in which the product of the SP, *S*, and electron energy, *E*, is plotted versus energy on a logarithmic scale. As examples, the solid circles in Figs. 1(a) and (b) show Fano plots of Si and Au using SPs calculated from optical data [17, 18] (hereafter referred to as optical SPs). Our Fano plots show optical SPs for energies between 10 eV and 100 eV to illustrate trends, although these SPs should be regarded only as semi-quantitative guides [18].

The nonrelativistic Bethe SP equation is [8-10]:

$$S = \frac{784.6\,Z\rho}{EA}\ln\left(\frac{1.166\,E}{I}\right) \qquad \text{(in eV/Å)}, \tag{1}$$

where Z is the atomic number, ρ is the density (in g/cm^3), A the atomic weight, I is the mean excitation energy (in eV), and E is expressed in eV. The dashed lines in Figs. 1(a) and (b) show plots of the product SE from Eq. (1) (with I values as recommended in Ref. [11]) as a function of E. While the Fano plots from the optical SPs for Si and Au show linear regions,

for energies greater than 500 eV for Si and greater than 10 keV for Au, their slopes are larger than those for the Fano plots from the Bethe equation. At lower energies, *SE* from the optical SPs gradually decrease and approach zero with decreasing energy. That is, as is well known, the Bethe SP equation is not valid for energies less than about 10 keV [11-18].

It is convenient to rearrange Eq. (1) for a Fano plot:

$$SEk = \ln(1.166/I) + \ln E \qquad \text{(in eV}^2\text{/Å)}, \qquad (2)$$

where $k = A/784.6Z\rho$. If the Bethe equation were valid over a given energy range, the corresponding plot of *SEk* versus ln*E* would be linear with a slope of unity.

The slopes of the Fano plots for Si and Au from the optical SPs are shown as solid circles in Figs.1 (c) and (d) as a function of electron energy. We see that these slopes show a series of steps with increasing energy. Each of these steps corresponds to contributions to the stopping power from a particular electronic shell (valence-band, L-shell, and K-shell for Si in Fig. 1(c) and valence-band, O-shell, N-shell, and M-shell for Au in Fig. 1(d)). As the energy increases to our limit of 30 keV, the slopes approach unity as expected from Eq. (2).

We have chosen to fit plots of slopes of Fano plots using the Hill equation [23]. In principle, any sigmoid function would be appropriate but the Hill equation is a simple expression that can be easily integrated. This equation can be expressed as

$$y = a\frac{E^n}{E^n + b^n}, \qquad (3)$$

where *a* is the height of a step, *b* is the electron energy at the center of a step, and *n* determines the steepness of the slope at a step. Although this equation is empirical, we can associate physical meanings to the parameters *a*, *b*, and *n*.

If a plot of the slope of a Fano plot for a given element has *m* steps, we can describe the plot by

$$k\frac{d(SE)}{d\ln E}=\sum_{i=1}^{m}a_i\frac{E^{n_i}}{E^{n_i}+b^{n_i}}. \qquad (4)$$

The solid lines in Figs. 1(c) and (d) show fits of the Fano-plot slopes for Si and Au with Eq. (4), and we see reasonable agreement. Although there are some deviations of the fits from the plotted points (e.g., for Si above 600 eV), these do not significantly affect our later results. We find it more convenient to fit the Fano plots directly with an integration of Eq. (4):

$$SE=\frac{784.6\,Z\rho}{A}\sum_{i=1}^{m}\left[\frac{a_i}{n_i}\ln\left(\frac{E^{n_i}+b^{n_i}}{b^{n_i}}\right)\right] \quad \text{(in eV}^2\text{/Å)}. \qquad (5)$$

We have fitted Fano plots with the optical SPs for our group of 41 elemental solids with Eq. (5). The solid lines in Figs. 2(a) and (b) show examples of these fits for Si and Au. Direct comparisons of the optical SPs and the values derived from the fits with Eq. (5) are shown in Figs. 2(c) and (d) where we see excellent agreement with the optical SPs. The root mean square (rms) difference of the fitted values from the optical values of *SE* were 0.8 % for Si and 1.0 % for Au. The average of the rms differences for the 41 solids was 1.0

% over the 100 eV to 30 keV energy range. This value is superior to those found in fits of the optical SPs with other empirical equations over the same energy range: 4.52 % with the Joy-Luo equation [14] and 3.04 % with the Jablonski-Tanuma-Powell [20] equation.

Our new expression for the SP can be obtained by rearranging Eq. (5):

$$S = \frac{784.6\,Z\rho}{EA}\sum_{i=1}^{m}\frac{a_i}{n_i}\ln\left[1+\left(\frac{E}{b_i}\right)^{n_i}\right] \qquad \text{(in eV/Å)}. \tag{6}$$

Values of the parameters in Eq. (6) for each of our 41 solids will be reported elsewhere [24]. For E much larger than all b_i, Eq. (6) becomes

$$S = \frac{784.6\,Z\rho}{EA}\sum_{i=1}^{m} a_i \ln\left(\frac{E}{b_i}\right) \qquad \text{(in eV/Å)}. \tag{7}$$

If a single electronic shell contributed to the SP (i.e., m = 1), Eq. (7) would become the Bethe SP equation (Eq. (1)) if a_1 = 1 and $b_1 = I/1.166$.

The optical SPs for 41 elements [17, 18] showed systematic changes as a function of atomic number. Multiple peaks and shoulders were seen with shapes and widths that varied with Z [18]. These changes were interpreted in terms of the varying contributions of valence-electron excitations and inner-shell excitations to the total SP. Our analysis of the optical SPs with the Hill equation has yielded insight into these separate contributions. The dashed lines in Figs. 2(a) and (c) show the valence-electron contributions to the SP for Si (i = 1), the L-shell contribution (i = 2), and the K-shell contribution (i = 3). While the electronic structure of Au is more complex than that of Si (with overlapping contributions from N- and O-

shells), we can similarly identify (at least approximately) the contributions of valence-electron excitations (i = 1), the O-shell (i = 2), the N-shell (i = 3), and the M-shell (i = 4) in Figs. 2(b) and (d).

We now consider the physical significance of the parameters in Eq. (6). Figure 3 shows plots of the b_i values derived from the fits of the optical SPs with Eq. (5) for the 41 solids as a function of binding energies of the K-shell and of the L_3-, M_3-, and N_3-subshells. We see clear near-linear dependences for b_K, b_L, b_M, and b_N, although there is larger scatter for the b_N plot in Fig. 3(d). The slopes of linear fits to the plots of Figs. 3(a), (b), (c), and (d) are 3.4, 3.4, 2.6, and 1.5, respectively. These slopes indicate that the values of b_i for a given element and shell can be regarded as an average excitation energy for that shell. It is reasonable that this average excitation energy should be roughly three times the corresponding inner-shell binding energy. The smaller slope found for the b_N plot in Fig. 3(d) is probably associated with the large range of binding energies for the various N subshells for medium- and high-Z elements and with the overlapping electronic excitations from N- and O-shells for high-Z elements.

The parameter a_i represents the height of a step in plots of the Fano-plot slopes such as Figs. 1(c) and (d). For E much larger than all b_i, the total of all step heights must be unity in order for the asymptotic slope to converge to the expected Bethe value (unity in the units of Figs. 1(c) and (d)). We found that the average value of the total step heights for the 41 solids was $\mathbf{1.08 \pm 0.07}$ (where the uncertainty represents one standard deviation). It is clear, however, from Figs. 1(c) and (d) that the Fano-plot slopes are decreasing with increasing

energy for $E > 10$ keV, and would become closer to unity for $E > 30$ keV. We can therefore regard the product a_iZ in Eqs. (6) and (7) as an effective number of electrons in each shell contributing to the stopping power.

The parameter n_i is a measure of the steepness of steps in plots of the Fano-plot slopes. Comparison of Figs. 1(c) and (d) shows that the steps for Si are relatively sharp while the steps for Au corresponding to the O-shell and N-shell steps are broader. These differences are qualitatively reasonable because of the large range of binding energies of the subshells, 57 eV to 762 eV, for the Au O-shell and N-shell [25].

In summary, we believe that Eq. (6) will be useful for Monte Carlo simulations of electron transport in solids that utilize the continuous slowing-down approximation for electron energies between 100 eV and 30 keV. Our fits of the optical SPs with the Hill equation have enabled us to identify the separate contributions of valence-band and inner-shell excitations to the stopping power, and of the trends in these contributions with Z.

References

[1] R. Gauvin, Surf. Interface Anal. 37 (2005) 875.

[2] N. W. M. Ritchie, Surf. Interface Anal. 37 (2005) 1006.

[3] X. Llovet, J. M. Fernández-Varea, J. Sempau, and F. Salvat, Surf. Interface Anal. 37 (2005) 1054.

[4] A. Jablonski, C. J. Powell, and S. Tanuma, Surf. Interface Anal. 37 (2005) 861.

[5] C. G. Frase and W. Häßler-Grohne, Surf. Interface Anal. 37 (2005) 942.

[6] J. S. Villarrubia, A. E. Vladár, and M. T. Postek, Surf. Interface Anal. 37 (2005) 951.

[7] D. V. Gorelikov, J. Remillard, N. T. Sullivan, and M. Davidson, Surf. Interface Anal. 37 (2005) 959.

[8] H. Bethe, Ann. Physik (Leipzig) 5 (1930) 325.

[9] H. Bethe, in: H. Geiger and K. Scheel (Ed.), Handbuch der Physik, Springer, Berlin, 1933, vol. 24/1, p. 273.

[10] H. A. Bethe and J. Ashkin, in: E. Segre (Ed.) Experimental Nuclear Physics, Wiley, New York, 1953, p. 166.

[11] Stopping Powers for Electrons and Positrons, International Commission on Radiation Units and Measurements Report No. 37, International Commission on Radiation Units and Measurements, Bethesda, 1984.

[12] M. J. Berger, J. S. Coursey, M. A. Zucker, and J. Chang, Stopping Power and Range Tables for Electrons, Positrons, and Helium Ions, (http://physics.nist.gov/PhysRefData/Star/Text/contents.html), 2005.

[13] T. S. Rao-Sahib and D. B. Wittry, J. Appl. Phys. 45 (1974) 5060.

[14] D. C. Joy and S. Luo, Scanning 11 (1989) 176.

[15] J. M. Fernández-Varea, R. Mayol, D. Liljequist, and F. Salvat, J. Phys.: Condens. Matter 5 (1993) 3593.

[16] D. C. Joy, http://web.utk.edu/~srcutk/htm/interact.htm.

[17] S. Tanuma, C. J. Powell, and D. R. Penn, Surf. Interface Anal (2005) 37, 978.

[18] S. Tanuma, C. J. Powell, and D. R. Penn, J. Appl. Phys. 103 (2008) 063707.

[19] D. R. Penn, Phys. Rev. B 35 (1987) 482.

[20] A. Jablonski, S. Tanuma, and C.J. Powell, J. Appl. Phys. 103 (2008) 063708.

[21] U. Fano, Phys. Rev. 95 (1954) 1198.

[22] M. Inokuti, Rev. Mod. Phys. 43 (1971) 297.

[23] A. V. Hill, J. Physiol. (Lond.) 40 (1910) iv.

[24] K. Kumagai, S. Tanuma, and C. J. Powell (to be published).

[25] NIST X-ray Photoelectron Spectroscopy Database, Version 3.5 (2008); http://srdata.nist.gov/xps.

Figure captions

Fig. 1. Fano plots ((a) and (b)) and slopes of Fano plots ((c) and (d)) for Si and Au. The closed circles are derived from optical SPs and the dashed lines in (a) and (b) show values from the Bethe equation [Eq. (1)]. The solid lines in (c) and (d) show fits to the Fano-plot slopes with Eq. (4), and the dashed lines indicate the value expected from the Bethe equation.

Fig. 2. The solid lines show fits of the Fano plots with the optical SPs (solid circles) using Eq. (5) for (a) Si and (b) Au. The solid circles in (c) and (d) are the optical SPs and the solid lines show the results of the fits. The dashed lines show the contributions of valence-band and inner-shell excitations to *SE* and *S*.

Fig. 3. Plots of values of b_i (solid circles) derived from fits of the Fano plots with Eq. (5) for the 41 elemental solids as a function of (a) K-shell, (b) L_3-subshell, (c) M_3-subshell, and (d) N_3-subshell binding energy. The solid lines show linear fits for each plot.

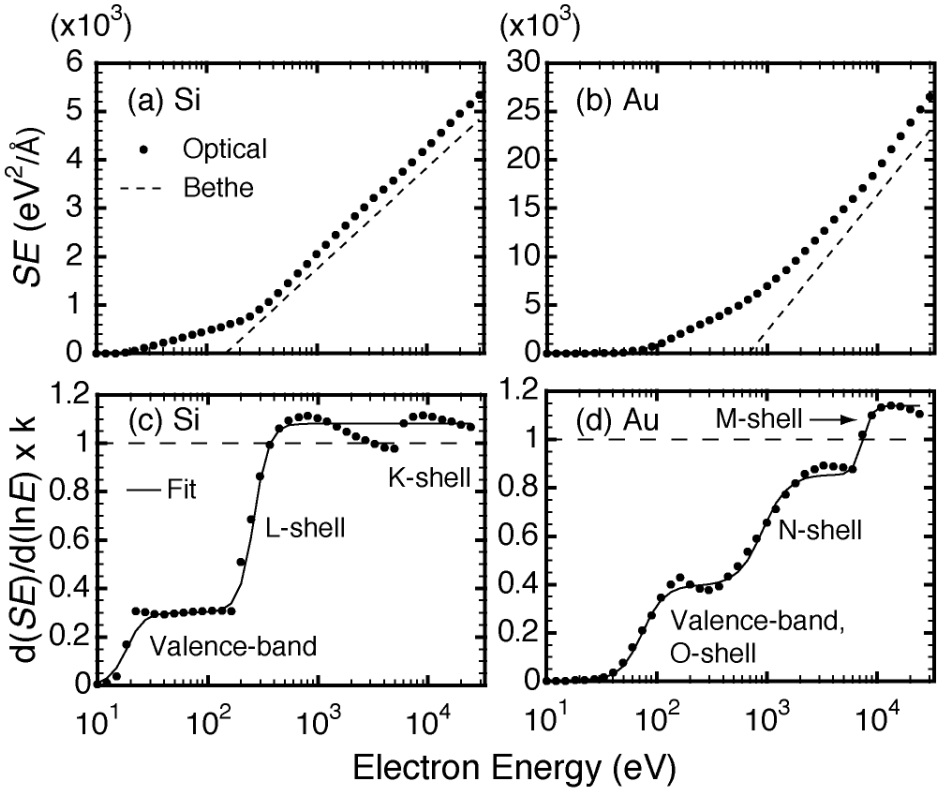
(x10^3)
(x10^3)
(a) Si
Optical
Bethe
(b) Au
SE (eV^2/Å)
(c) Si
Fit
K-shell
L-shell
Valence-band
(d) Au
M-shell
N-shell
Valence-band,
O-shell
d(SE)/d(lnE) x k
Electron Energy (eV)

Fig.1.

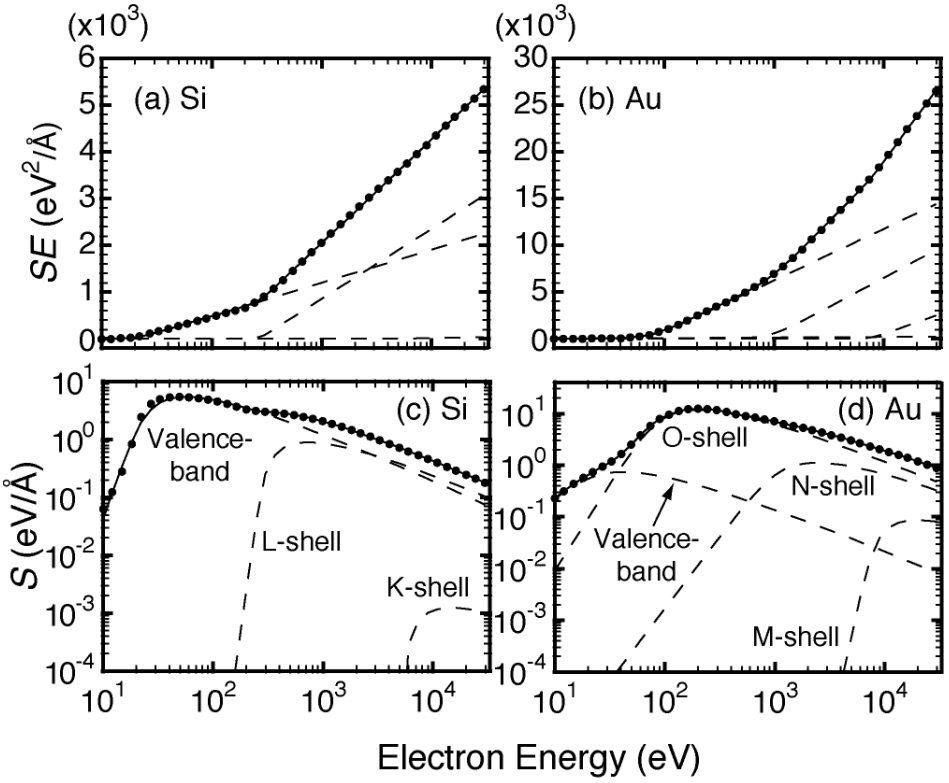
(x10^3)
(x10^3)
(a) Si
(b) Au
SE (eV^2/Å)
(c) Si
(d) Au
Valence-band
L-shell
K-shell
O-shell
N-shell
Valence-band
M-shell
S (eV/Å)
Electron Energy (eV)

Fig.2.

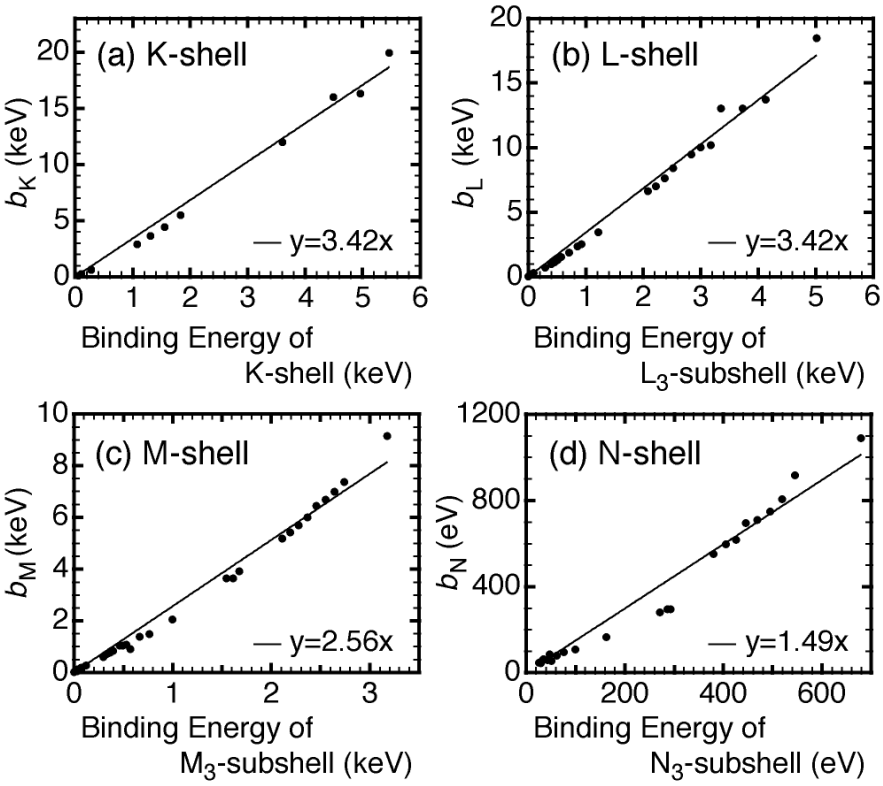
(a) K-shell
b_K (keV)
— y=3.42x
Binding Energy of
K-shell (keV)
(b) L-shell
b_L (keV)
— y=3.42x
Binding Energy of
L_3-subshell (keV)
(c) M-shell
b_M (keV)
— y=2.56x
Binding Energy of
M_3-subshell (keV)
(d) N-shell
b_N (eV)
— y=1.49x
Binding Energy of
N_3-subshell (eV)

Fig.3.